

# Identification of new nearby white dwarfs using *Gaia* DR3

Alex Golovin<sup>1</sup>\*, Sabine Reffert<sup>1</sup>, Akash Vani<sup>2</sup>, Ulrich Bastian<sup>2</sup>, Stefan Jordan<sup>2</sup>, and Andreas Just<sup>2</sup>

<sup>1</sup> Landessternwarte, Zentrum für Astronomie der Universität Heidelberg, Königstuhl 12, 69117 Heidelberg, Germany

<sup>2</sup> Astronomisches Rechen-Institut, Zentrum für Astronomie der Universität Heidelberg, Mönchhofstr. 12–14, 69120 Heidelberg, Germany  
e-mail: agolovin@lsw.uni-heidelberg.de

Version: December 20, 2023

## ABSTRACT

**Context.** A volume-complete sample of white dwarfs is essential for statistical studies of the white dwarf population. The sample of nearby white dwarfs is the only one that allows the faint end of the luminosity function to be probed and thus is the only one that covers the entire range of white dwarf ages. However, due to their intrinsic faintness, even nearby white dwarfs are difficult to identify.

**Aims.** Our work focuses on improving the completeness and purity of the white dwarf census within 50 pc of the Sun. To accomplish this, we used *Gaia* Data Release 3 (*Gaia* DR3) to identify and characterise new and previously overlooked white dwarfs in the solar neighbourhood. We also identify objects with spurious astrometric solutions in *Gaia* DR3 but claimed as high-confidence white dwarfs in the *Gaia* Catalogue of White Dwarfs (GCWD21) by Gentile Fusillo et al. (2021).

**Methods.** Based on the astrometry and photometry in *Gaia* DR3, we identified new nearby white dwarfs and validated those that had been missed from recent white dwarf catalogues despite being previously documented. To ensure the reliability of their astrometric solutions, we used a cut on just two parameters from *Gaia* DR3: the amplitude of the image parameter determination goodness-of-fit and the parallax-over-error ratio. In addition, we imposed photometric signal-to-noise requirements to ensure the reliable identification of white dwarfs when using the colour-magnitude diagram.

**Results.** We have identified nine previously unreported white dwarfs within the local population of 50 pc, and validated 21 previously reported white dwarfs missing from the GCWD21 and other recent volume-limited white dwarf samples. A few of these objects belong to the rare class of ultra-cool white dwarfs. Four white dwarfs in our sample have an effective temperature of  $T_{\text{eff}} \leq 4000$  K within the  $1\sigma$  interval, and two of them have an absolute magnitude of  $M_G > 16.0$  mag. The identified white dwarfs are predominantly located in crowded fields, such as near the Galactic plane or in the foreground of the Large Magellanic Cloud. We also find that 19 of these white dwarfs have common proper motion companions with angular separations ranging from 1.1'' to 7.1'' and brightness differences between the components of up to 9.8 magnitudes. One of these systems is a triple system consisting of a white dwarf and two K dwarfs, while another is a double white dwarf system. The identified white dwarfs represent a 1.3% improvement in the completeness of the 50 pc sample, resulting in a new total of 2265 known white dwarfs located within 50 pc of the Sun. We have identified 103 contaminants among the 2338 high-confidence white dwarfs in the 50 pc subsample of the GCWD21 and have found that their astrometric solutions in *Gaia* DR3 are spurious, improving the purity by 4.4%.

**Key words.** White dwarfs – Stars: distances – Hertzsprung-Russell and C-M diagrams – solar neighbourhood – Astrometry – Galaxy: stellar content

## 1. Introduction

The vast majority of stars in the solar neighbourhood will end their evolutionary path as white dwarfs. Statistical studies of the white dwarf population provide insights into the stellar formation history of the solar neighbourhood (Yuan 1992; Rowell 2013; Isern 2019). The luminosity function of white dwarfs allows us to infer the age of the local stellar population (Schmidt 1959; Liebert et al. 1979, 1988; Yuan 1992; Harris et al. 2006; Catalán et al. 2008) and can even help in the search for evidence of dark matter, by constraining the properties of hypothetical dark matter particles, such as axions (Isern et al. 2008).

However, due to the intrinsic faintness of white dwarfs, the sample of nearby white dwarfs in the solar neighbourhood is the only sample that contains the full range of white dwarf ages. If the sample is incomplete, the derived luminosity function may be biased. Discoveries of nearby white dwarfs can have a significant

impact on the statistical properties of the luminosity function, its shape, and in particular the position of the cutoff at the faint end, which is defined by the age of the oldest white dwarfs in the solar neighbourhood. Besides increasing the completeness of the sample, such discoveries may improve the accuracy of the luminosity function, thus providing a better understanding of our Galaxy and its history.

Furthermore, the high completeness of the local white dwarf census is important for selecting suitable targets for studies of individual objects. For instance, McGill et al. (2018) predicted an astrometric microlensing event caused by the nearby white dwarf GJ 440 (= LAWD 37) by using *Gaia* Early Data Release 3 (EDR3; Gaia Collaboration et al. 2021a; Lindgren et al. 2021). Subsequently, they confirmed this event using the *Hubble* Space Telescope, which allowed them to directly obtain the mass of GJ 440 through gravitational microlensing (McGill et al. 2023). This was the first time such a measurement had been made for a single star other than the Sun from a predicted astrometric microlensing event.

\* Fellow of the International Max Planck Research School for Astronomy and Cosmic Physics at the University of Heidelberg (IMPRS-HD)

When hunting for white dwarfs that may have been overlooked in previous studies, it is reasonable to expect that they are likely hidden in the densest part of the Galactic plane, which is often avoided by surveys due to high source density, such as RAVE (Steinmetz et al. 2020), GALAH (De Silva et al. 2015), and SEGUE (Yanny et al. 2009). White dwarfs can also go unnoticed when they are paired with a considerably brighter companion in a binary system, which outshines them and makes them challenging to detect (Ferrario 2012).

The *Gaia* Catalogue of White Dwarfs (Gentile Fusillo et al. 2021, hereafter referred to as the GCWD21) is based on *Gaia* EDR3 and lists 359 073 high-confidence white dwarfs with a probability,  $P_{\text{WD}}$ , of being a white dwarf greater than 0.75. The selection criteria used to identify these white dwarfs are complex and described in Eqs. 1–21 of Gentile Fusillo et al. (2021). These selection criteria include cuts on the photometric excess factor, which is based on photometry alone (Evans et al. 2018; Lindegren et al. 2018), and a conservative cut on the re-normalised unit weight error (RUWE), whose re-normalisation factor is also a function of the *G*-band magnitude and the  $BP - RP$  colour (Lindegren 2018).

The completeness of the local white dwarf census can be further improved by applying selection criteria based solely on astrometry rather than employing cuts that involve both astrometry and photometry in *Gaia* DR3. When constructing the Fifth Catalogue of Nearby Stars (CNS5), Golovin et al. (2023) demonstrated that a cut on the amplitude of angular variation of the image parameter determination goodness-of-fit (IPD GoF; `ipd_gof_harmonic_amplitude` in *Gaia* EDR3 and *Gaia* DR3) effectively eliminates sources with spurious astrometric solutions. This cut (Eq. (2) of this paper), when applied to nearby sources, outperforms the commonly used cut on RUWE. The IPD GoF cut is based solely on astrometry and is independent of the object’s magnitudes. This approach allows the recovery of objects that have reliable parallaxes but with peculiarities in their photometry, hence increasing sample completeness. The cut was validated and discussed in detail in Golovin et al. (2023). More recently, Vani et al. (in preparation) demonstrated that this approach is effective even for distances beyond 25 pc. On the other hand, 50 pc is the distance limit at which parallaxes of white dwarfs are measured with a relative uncertainty of 5% or better, given that the 95th percentile of the *Gaia* parallax uncertainty for white dwarfs in the GCWD21 is 1 mas. The GCWD21 contains 2338 white dwarfs that are possibly located within 50 pc of the Sun.

In this paper we report the identification of nine new white dwarfs in the 50 pc local population using *Gaia* DR3. The white dwarfs that have been identified (referred to as ‘new white dwarfs’ hereafter) were not included in the GCWD21. Additionally, they are not listed in the Montreal White Dwarf Database<sup>1</sup> (Dufour et al. 2017) and were omitted in previous white dwarf studies that relied on *Gaia* DR3. Therefore, these newly identified white dwarfs are also missing from the recent volume-limited white dwarf samples (e.g. Fleury et al. 2022; Torres et al. 2022; Cukanovaite et al. 2023; Jiménez-Esteban et al. 2023; Vincent et al. 2023; O’Brien et al. 2023; Torres et al. 2023). In addition, our selection validated 21 white dwarf candidates that are missing from the GCWD21 and the samples mentioned above but designated as white dwarfs in El-Badry et al. (2021) or in O’Brien et al. (2023) or listed in the *Gaia* Catalogue of Nearby Stars (GCNS; Gaia Collaboration et al. 2021b) with a probability of being a white dwarf greater than 0.75.

It is noteworthy that most of these objects have been previously identified as nearby stars. Specifically, 27 of them are included in the GCNS, and four of them are listed in the CNS5 catalogue. However, they have not been identified as white dwarfs in these catalogues, with the exception of three objects with higher white dwarf probabilities in the GCNS.

Finally, among the 2338 high-confidence white dwarfs in the 50 pc subsample of the GCWD21, we have identified 103 contaminants whose astrometric solutions in *Gaia* DR3 are most likely spurious. We argue that these objects should be omitted from the 50 pc sample.

This paper is organised as follows. In Sect. 2 we describe our selection criteria. Section 3 presents newly identified white dwarfs in the 50 pc local population. The stellar parameters of the identified white dwarfs are reported in Sect. 4. In Sect. 5 we focus on improving the purity of the local white dwarf census. Section 6 provides our conclusions and a summary, and in Appendix A we discuss the discrete source classifier (DSC) of the white dwarfs in *Gaia* DR3.

## 2. Data selection in *Gaia* DR3

To identify new white dwarfs, we constructed a primary sample by retrieving all the objects that are possibly located within 50 pc of the Sun from *Gaia* DR3:

$$\varpi_{\text{DR3}} + 3 \sigma_{\varpi_{\text{DR3}}} \geq 20 \text{ mas}, \quad (1)$$

where  $\varpi_{\text{DR3}}$  denotes the measured parallax in the *Gaia* DR3 catalogue and  $\sigma_{\varpi_{\text{DR3}}}$  is its uncertainty.

In *Gaia* DR3, the amplitude of angular variation of the IPD GoF indicates the degree of asymmetry in the image. This parameter allows us to distinguish single stars from sources with asymmetric images, such as poorly resolved binaries or mismatched sources (two or more different sources assigned to the same `source_id`, resulting in a spurious catalogue entry).

We eliminated spurious sources or those with unreliable astrometry by applying a cut on the amplitude of the IPD GoF in *Gaia* DR3 originally introduced by Golovin et al. (2023). For the reader’s convenience, we restate this condition here:

$$A_{\text{GoF}} < 10^{-5.12} (\varpi_{\text{DR3}} / \sigma_{\varpi_{\text{DR3}}})^{2.61}, \quad (2)$$

where  $A_{\text{GoF}}$  is the amplitude of the IPD GoF (`ipd_gof_harmonic_amplitude`). The cut parameters are chosen to separate the two groups formed by sources with reliable and spurious astrometric solutions in the ( $A_{\text{GoF}}, \varpi_{\text{DR3}} / \sigma_{\varpi_{\text{DR3}}}$ ) parameter space (Fig. 1). This selection criterion has been validated in Golovin et al. (2023) against the machine learning classifier from Rybizki et al. (2022), the classifier from Gaia Collaboration et al. (2021b), which was used to generate the GCNS, and the negative parallax sample.

To ensure the reliable identification of white dwarfs based on their position in the colour-magnitude diagram (CMD), we required that the *G*-, *BP*-, and *RP*-band photometry have a sufficiently high signal-to-noise ratio:

$$\left. \begin{array}{l} \text{(i) } \text{phot\_g\_mean\_flux\_over\_error} > 20 \\ \text{(ii) } \text{phot\_bp\_mean\_flux\_over\_error} > 20 \\ \text{(iii) } \text{phot\_rp\_mean\_flux\_over\_error} > 20 \end{array} \right\}. \quad (3)$$

Furthermore, we augmented our sample by including objects that have photometry with a lower signal-to-noise ratio. How-

<sup>1</sup> <https://www.montrealwhitedwarfdatabase.org/home.html>

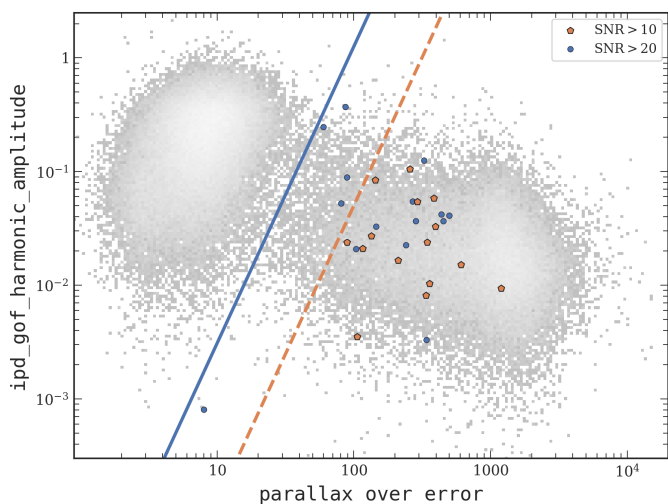


**Fig. 1.** Amplitude of angular variation in the IPD GoF as a function of  $|\varpi/\sigma_\varpi|$  for white dwarfs in this work (blue and orange symbols). The blue line corresponds to Eq. (2); the orange dashed line corresponds to the cut defined in Eq. (4)-(iv) to select objects with lower S/N in photometry (orange pentagons). For comparison, the 50 pc *Gaia* DR3 sample is shown in the background (grey symbols).

ever, for these objects, we imposed a more conservative requirement on the IPD GoF amplitude in *Gaia* DR3:

$$\left. \begin{array}{l} \text{(i) } \text{phot\_g\_mean\_flux\_over\_error} > 10 \\ \text{(ii) } \text{phot\_bp\_mean\_flux\_over\_error} > 10 \\ \text{(iii) } \text{phot\_rp\_mean\_flux\_over\_error} > 10 \\ \text{(iv) } A_{\text{GoF}} < 10^{-6.52} (\varpi_{\text{DR3}}/\sigma_{\varpi_{\text{DR3}}})^{2.61} \end{array} \right\}. \quad (4)$$

It should be noted that sources with a flux-over-error ratio  $< 10$  are affected by the low flux threshold issue in *Gaia*, resulting in a clipped distribution of their fluxes in epoch photometry at the faint end, which leads to an overestimated mean flux (Riello et al. 2021; Fabricius et al. 2021). This issue predominantly affects the *BP* band, as the majority of sources have lower fluxes in *BP* compared to the *RP* band. Consequently, the faint end of the main sequence on the CMD bends towards bluer colours, becoming statistically indistinguishable from the faint end of the white dwarf sequence.

In this study, we opted to use the  $(G, BP - RP)$  parameter space to mitigate the impact of blending and contamination in photometry on our analysis. Although the  $G - RP$  colour is often favoured for its typically higher signal-to-noise ratio as compared to the  $BP - RP$  colour (e.g. Scholz 2020; Kaltenecker & Faherty 2021; Reylé et al. 2023; Jiménez-Esteban et al. 2023), it is prone to blending of faint sources, particularly in crowded fields. In *Gaia*, blending primarily affects the *BP* and *RP* fluxes rather than the *G* band because of the very different window sizes used in the photometric instrument and the astrometric field CCD (Busso et al. 2021). Consequently, blended objects appear redder than expected in the CMD when the  $G - RP$  colour is used (see Golovin et al. 2023 for further details).

The CMD provides a reliable means of identifying white dwarfs in the solar neighbourhood, given the distinct position of their sequence and the availability of extremely precise astrometry from *Gaia* DR3. We employed the following cut to select objects located in the white dwarf region on the CMD:

$$\left. \begin{array}{l} \text{(i) } M_G > 10 \text{ mag} + 2.5 (BP - RP) \\ \text{(ii) } BP - RP < 1.9 \text{ mag} \end{array} \right\}, \quad (5)$$

where  $M_G$  represents the object’s absolute magnitude in the *G* band, calculated as  $M_G = \text{phot\_g\_mean\_mag} + 5 \log_{10}(\varpi_{\text{DR3}} [\text{mas}]/100)$ . This cut is shown by the dotted line in Fig. 2.

As a final step, we cross-matched our resulting sample, consisting of 2250 objects, with the GCWD21 catalogue. Subsequently, we excluded 2220 objects that are already listed in the GCWD21 catalogue. This left 30 objects. These objects are examined in more detail in the following section.

It is important to emphasise that our selection criteria solely employ the *Gaia* DR3 content that was already available in *Gaia* EDR3. Consequently, the selection process using either *Gaia* EDR3<sup>2</sup> or *Gaia* DR3 leads to the same resulting samples.

### 3. White dwarf sample

#### 3.1. New and validated white dwarfs within 50 pc

We identified 30 new or so far overlooked white dwarfs within 50 pc with exquisite astrometry in *Gaia* DR3, following the criteria outlined in Sect. 2. In Fig. 2 we show the location of these white dwarfs on the CMD, as well as their common proper motion (CPM) companions (see Sect. 3.2). Their astrometric and photometric properties are summarised in Table 1. In total, 21 of these white dwarfs have been previously documented as such at least once, but are missing from the GCWD21 and recent volume-limited white dwarf samples. The remaining nine objects in our list are new white dwarfs that were not previously reported as members of this class.

According to the DSC of white dwarfs in *Gaia* DR3, all these 30 objects have probabilities lower than 0.5 for being categorised as white dwarfs. However, prior research has shown the shortcomings of this classifier, highlighting its limited purity and sub-optimal performance (Creevey et al. 2023; Ulla et al. 2022). Notably, the sudden decline in inferred probabilities coincides with  $BP - RP = 0.6$  mag, corresponding to a flux ratio of  $I_{RP}/I_{BP} = 1$  (see Appendix A for more details).

After cross-matching our list with Pan-STARRS1 (PS1; Chambers et al. 2016), we found that five objects in our list have a counterpart in PS1. Combining photometry from PS1 with extremely accurate astrometry from *Gaia* DR3 further supports that these objects are indeed white dwarfs. The position of these objects on the CMD perfectly overlaps with the white dwarf cooling sequence, as shown in Fig. 3. Notably, one of these objects (*Gaia* DR3 4314988445029569920 = PS1 122052927423559882) even appears to be one of the reddest white dwarfs in the solar neighbourhood. Although not the reddest in terms of  $BP - RP$  colour, this white dwarf is also the faintest in our sample in terms of absolute *G*-band magnitude. We estimated its effective temperature to be about  $T_{\text{eff}} \sim 3700$  K by fitting the Montreal models to *Gaia* DR3 and PS1 photometry (see Sect. 4 for details). This suggests that this object is potentially one of the oldest and coldest white dwarfs in the local population, placing it in the rare class of ultra-cool white dwarfs.

#### 3.2. Common proper motion companions

For 19 white dwarfs in our list, we identified CPM companions in *Gaia* DR3 by selecting pairs with statistically identical parallaxes, proper motions consistent with a Keplerian orbit, and

<sup>2</sup> Even though in this particular case the resulting samples will be the same, for sources with 6-p astrometric solutions in *Gaia* EDR3 a correction to the *G*-band photometry has to be applied (Riello et al. 2021). In *Gaia* DR3 these corrections are already included.

**Table 1.** New and validated white dwarfs within 50 pc and their parameters from *Gaia* DR3. For counterparts in Pan-STARRS1, the PS1\_id is given. The last column lists references where the object has been reported as a white dwarf.

<i>Gaia</i> DR3 source_id	$\alpha_{2016.0}$ [deg]	$\delta_{2016.0}$ [deg]	$\varpi$ [mas]	$\sigma_{\varpi}$ [mas]	$\mu_{\alpha*}$ [mas yr <sup>-1</sup> ]	$\sigma_{\mu_{\alpha*}}$ [mas yr <sup>-1</sup> ]	$\mu_{\delta}$ [mas yr <sup>-1</sup> ]	$\sigma_{\mu_{\delta}}$ [mas yr <sup>-1</sup> ]	$G$ [mag]	$\sigma_G$ [mag]	$BP - RP$ [mag]	$\sigma_{BP-RP}$ [mag]	PS1_id	Reference <sup>a</sup>
601364766939138688	232.34488	-35.87226	56.76	0.95	2.66	0.37	2.01	0.44	17.3027	0.0036	1.354	0.011		This work
4651329704762754944	79.00237	-72.23388	44.802	0.090	-61.54	0.10	812.23	0.12	14.60519	0.00093	0.724	0.049		1
6017724140666000896	247.87332	-39.01564	44.46	0.11	-417.61	0.15	-308.31	0.15	16.6801	0.0057	1.073	0.077		1
298325662868370048	79.99882	-15.83773	42.279	0.035	182.685	0.031	216.203	0.32	14.3316	0.0016	0.60	0.15		1
1938960722332184704	355.69590	46.15057	37.08	0.43	-2.25	0.23	-9.11	0.39	17.0716	0.0016	0.756	0.047	163383556957661286	This work
2078105327586616832	295.44066	43.74985	36.73	0.11	61.28	0.15	72.55	0.18	17.4825	0.0036	1.20	0.12		1
6119354336882826752	214.60295	-36.55506	35.965	0.083	-17.988	0.096	-19.642	0.094	16.9170	0.0017	1.650	0.065		This work
2831490694928280576	346.63271	19.91053	34.020	0.10	281.90	0.15	-1.409	0.098	15.0260	0.0025	0.529	0.061		1
5956907713001974656	268.21937	-41.99552	31.512	0.097	145.58	0.11	-172.515	0.10	15.8141	0.0043	0.541	0.10		1
6665685378201412992	299.06923	-52.97232	31.319	0.081	141.86	0.12	-73.72	0.11	16.3813	0.0029	0.83	0.10		1, 2
205635204411687168	76.71714	44.44491	29.585	0.065	13.402	0.072	6.695	0.062	16.5293	0.0013	1.041	0.057		1
2651214734078859648	346.61426	-0.49425	28.33	0.20	-383.12	0.15	-244.34	0.13	16.4721	0.0020	1.44	0.11		This work
4110515669211359744	262.19720	-24.15883	26.89	0.30	-265.23	0.36	-293.65	0.24	17.7038	0.0021	1.383	0.020		This work
5463514273884166016	150.15300	-30.68801	26.277	0.090	77.660	0.067	37.642	0.094	17.0753	0.0028	1.054	0.075	79012621975390142	This work
6566046912935892352	325.76201	-75.12733	24.988	0.088	-23.094	0.094	425.34	0.12	18.0312	0.0013	1.210	0.033		This work
6063480282704764928	198.77439	-56.54848	24.77	0.31	-31.24	0.19	-259.62	0.23	18.3635	0.0030	0.65	0.10		2, 3, 4
1355203232910297600	257.96584	43.26073	24.528	0.040	-112.197	0.048	-184.413	0.047	16.22051	0.0018	1.771	0.015		This work
253360345315705344	18.70369	-0.97166	23.702	0.092	-22.41	0.11	203.772	0.073	14.2693	0.0029	-0.04	0.10		1
4663902104803506816	76.72861	-64.81502	22.970	0.096	306.58	0.13	108.81	0.12	18.0639	0.0015	1.076	0.023		3
3462945170562185088	183.23736	-34.08703	22.11	0.21	100.03	0.22	-164.90	0.21	18.7238	0.0066	1.43	0.11		1
6080038412403680256	197.61442	-52.99006	21.882	0.064	-100.018	0.069	13.532	0.058	16.6650	0.0013	1.082	0.069		1
2021862490380335232	294.58601	25.69982	21.65	0.19	58.58	0.28	-1.76	0.26	17.6669	0.0077	0.760	0.074		This work
6039626481000400128	238.17214	-31.86765	21.20	0.15	-125.28	0.16	26.29	0.10	17.8826	0.0045	0.887	0.020		1
6039626481009257472	238.17232	-31.86738	21.14	0.16	-132.03	0.17	41.05	0.11	17.9793	0.0019	0.995	0.096		1
4837326390227065344	63.93907	-45.97118	20.710	0.077	245.026	0.076	-129.57	0.12	16.7347	0.0024	0.671	0.064		1
1323632298413108096	241.81026	34.02664	20.504	0.057	96.269	0.065	-5.02	0.11	16.5644	0.0015	0.642	0.089		1
4468278954501360128	272.03420	1.87819	19.87	0.22	-22.35	0.24	36.11	0.23	18.3603	0.0031	1.466	0.069	110252720342434261	1
625602672887745152	155.17523	20.46312	19.73	0.19	-160.20	0.21	-188.34	0.22	18.4834	0.0035	0.991	0.062	132551551754976643	3
4314988445029569920	292.74236	11.71608	19.2	2.4	11.8	1.6	-16.1	1.5	19.9190	0.0094	1.362	0.043	122052927423559882	This work

<sup>a</sup> 1 - El-Badry et al. (2021), 2 - O'Brien et al. (2023), 3 - Gaia Collaboration et al. (2021b), 4 - Gentile Fusillo et al. (2019)

**Table 2.** CPM companions to the white dwarfs identified in this work.

WD	CPM companion	$\varpi$	$\sigma_{\varpi}$	$\mu_{\alpha^*}$	$\sigma_{\mu_{\alpha^*}}$	$\mu_{\delta}$	$\sigma_{\mu_{\delta}}$	$G$	$BP - RP$	SpT	$\rho$	$s$
<i>Gaia</i> DR3 source_id	<i>Gaia</i> DR3 source_id	[mas]	[mas]	[mas yr <sup>-1</sup> ]	[mas yr <sup>-1</sup> ]	[mas yr <sup>-1</sup> ]	[mas yr <sup>-1</sup> ]	[mag]	[mag]		["]	[AU]
4651329704762754944	4651329704762754176	44.856	0.016	-46.932	0.018	825.909	0.022	10.755	2.357	M1.5V	2.98	66.5
6017724140666000896	6017724140678769024	44.373	0.049	-429.581	0.054	-330.311	0.044	7.057	1.059	G9V	7.14	160.8
298325662868370048	298325662869643776	42.116	0.016	173.704	0.014	207.709	0.014	8.394	1.250	K4V	3.65	86.5
2078105327586616832	2078105327586616704	36.644	0.018	50.702	0.021	75.325	0.019	7.762	0.937	K0V	6.54	178.3
6119354336882826752	6119354336882826880	36.189	0.023	-34.259	0.027	-22.779	0.028	12.173	2.460	M3V	2.55	70.9
2831490694928280576	2831490694929214464	34.115	0.019	286.890	0.023	5.057	0.017	6.314	0.700	F8V	5.24	154.1
6665685378201412992	6665685343840128384	31.494	0.015	134.355	0.014	-74.846	0.012	10.009	1.696	K7V	6.83	217.17
5956907713001974656	5956907713041688960	31.361	0.026	140.745	0.028	-190.891	0.018	6.061	0.710	F6V	4.90	156.6
205635204411687168	205635200112139520	29.550	0.019	15.824	0.022	24.176	0.018	11.778	2.237	M2V	2.85	96.5
2651214734078859648	2651214734078859776	28.378	0.024	-376.420	0.024	-238.486	0.020	11.667	2.355	M1.5V	2.21	78.1
6566046912935892352	6566046809856626944	25.168	0.023	206.609	0.018	-62.312	0.021	6.554	0.688	F6V	5.62	226.05
1355203232910297600	1355203232910297728	24.557	0.014	-101.075	0.016	-185.807	0.016	12.713	2.273	M2.5V	2.15	87.7
2533660345315705344	2533660345315782528	23.539	0.087	-14.263	0.099	205.414	0.060	5.582	0.608	F0V	5.99	253.5
3462945170562185088	3462945170563600640	21.894	0.020	107.608	0.021	-166.659	0.021	12.972	2.294	M2.5V	3.52	159.5
6080038412403680256	6080038408112210176	21.837	0.017	-98.057	0.015	23.998	0.014	12.318	2.204	M1.5V	2.59	118.6
6039626481009257472	6039626481000400128	21.20	0.15	-125.28	0.16	26.29	0.10	17.883	0.887	-	1.13	53.5
4837326390227065344	4837326385930314368	20.707	0.012	242.804	0.012	-123.338	0.017	8.728	0.942	G9V	4.65	224.8
1323632298413108096	1323632508865678080	20.551	0.011	95.297	0.010	-2.102	0.013	10.432	1.577	K6V	4.55	222.0
4468278954501360128	4468275995268525056	20.397	0.014	-16.585	0.014	40.233	0.013	12.001	1.860	M0.5V	5.48	275.7

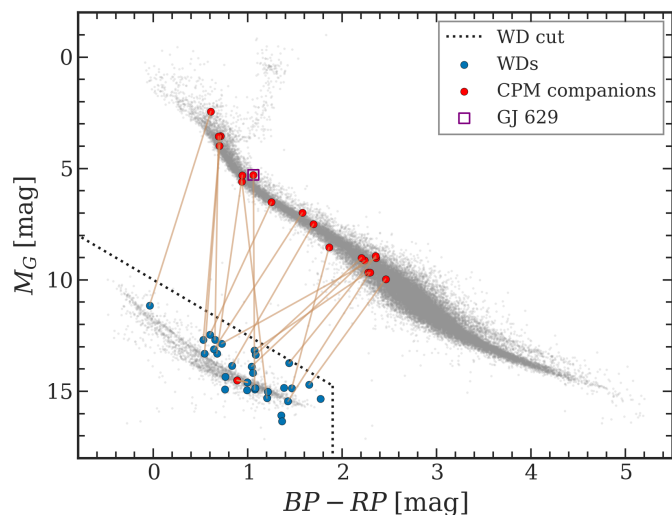


**Fig. 2.** *Gaia* DR3 CMD for the identified white dwarfs (blue symbols) and their CPM companions (red symbols). The adopted cut on the white dwarf locus is indicated by the dotted line. The solid orange lines connect white dwarfs to their corresponding CPM companions. Note that one of the pairs is a double white dwarf system (red symbol below the dotted line). For comparison, the CMD for the 50 pc *Gaia* DR3 sample is shown in the background (grey symbols). The square symbol indicates GJ 629, which is itself a spectroscopic binary (see Sect. 3.2 for details).

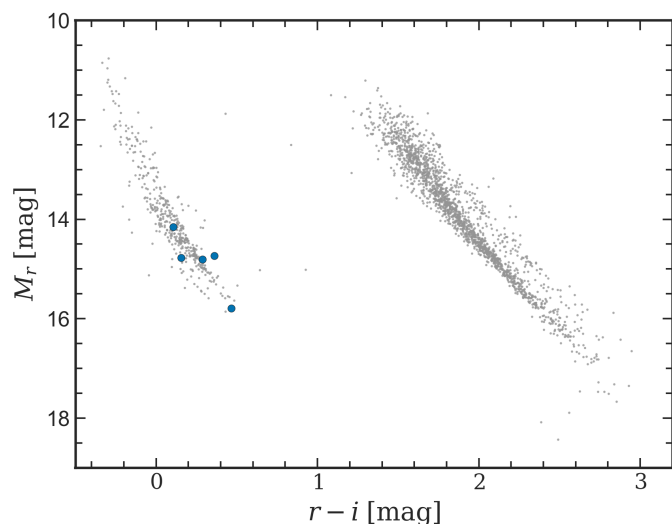


**Fig. 3.** PS1 CMD of the five counterparts for the identified white dwarfs. For illustrative purposes, the CMD for the 50 pc sample is displayed in the background (grey points), containing only objects that have at least 10 detections in  $r$  and  $i$  PS1 bands, and magnitude uncertainties below 0.01 mag.

projected separations of less than 1 pc (see El-Badry et al. 2021 for details). The identified binaries have angular separations  $\rho$  ranging from 1.1'' to 7.1'' and projected separations  $s$  between 54 and 276 AU. To estimate the spectral types of the main-sequence CPM companions, we used their absolute magnitudes  $M_G$  and relied on the empirical  $M_G$  and spectral type sequence from Pecaut & Mamajek (2013)<sup>3</sup>. We list the astrometric parameters of the CPM companions from *Gaia* DR3 along with their

spectral types and angular and projected separations in Table 2. Their positions on the CMD are shown in Fig. 2, denoted by red symbols.

One of the identified CPM pairs turned out to be a double white dwarf system, as the CPM companion to *Gaia* DR3 6039626481000400128 is another white dwarf from our list (*Gaia* DR3 6039626481009257472). Assuming a circular orbit and that the projected separation of this system is equal to its true semi-major axis, this corresponds to an orbital period of  $P \sim 375$  yr.

In addition to providing single-star astrometric solutions, *Gaia* DR3 also incorporates non-single-star (NSS) solutions for astrometric and spectroscopic binaries (Halbwachs et al. 2023; Holl et al. 2023b). Notably, in this data release only unresolved binaries were considered for the NSS processing (Pourbaix et al. 2022).

Of all the white dwarfs and their CPM companions identified in this work, only one object, namely GJ 629 (= *Gaia* DR3 6017724140678769024), which is the CPM companion of *Gaia* DR3 6017724140666000896, has an entry in the NSS tables of *Gaia* DR3 indicating that GJ 629 is a spectroscopic binary itself. This suggests that *Gaia* DR3 6017724140666000896 and GJ 629 constitute a triple system. Although it has been demonstrated that some of the listed NSS solutions in *Gaia* DR3 may be spurious and not all objects with NSS-solutions represent genuine binaries (Spaeth et al. 2023), as well as that scan-angle-dependent signals in *Gaia* DR3 can lead to spurious periods (Holl et al. 2023a), it is important to note that it had been already established before *Gaia* DR3 that GJ 629 is a spectroscopic binary, consisting of two early-K dwarfs (Bopp et al. 1970; Raghavan et al. 2010; Pourbaix et al. 2004; Fuhrmann et al. 2017). Furthermore, the orbital period of  $P = 31.8$  d obtained from the NSS-solution in *Gaia* DR3 is consistent with previously reported values (Bopp et al. 1970; Raghavan et al. 2010). Remarkably, GJ 629 is also the only main-sequence companion that lies photometrically in the main-sequence binary band of Fig. 2.

Regarding the remaining objects in our list, their astrometric solutions are consistent with a single-star model, and there is no evidence supporting the existence of additional components orbiting these objects.

#### 4. Stellar parameters

The ultra-precise parallaxes available from *Gaia* DR3, along with multi-colour photometry, enable us to estimate the stellar parameters of the identified white dwarfs. This is accomplished by photometric fitting of the Montreal DA (pure hydrogen) and DB (pure helium) models<sup>4</sup> (Bédard et al. 2020) to the spectral energy distribution of a white dwarf. The photometric fitting was performed with the WDPHOTools package (Lam et al. 2022) utilising the Markov chain Monte Carlo method to sample the posterior distribution of the inferred parameters, such as effective temperature  $T_{\text{eff}}$ , surface gravity  $\log(g)$ , mass  $M$ , and bolometric magnitude  $M_{\text{bol}}$ .

The input parameters required by the WDPHOTools for the photometric fitting include the type of atmosphere and fluxes in different photometric bands along with their associated uncertainties. As the atmospheric compositions are unknown, we obtained both DA and DB solutions for each white dwarf in our

<sup>3</sup> updates available at [https://www.pas.rochester.edu/~emamajek/EEM\\_dwarf\\_UBVJHK\\_colors\\_Teff.txt](https://www.pas.rochester.edu/~emamajek/EEM_dwarf_UBVJHK_colors_Teff.txt)

<sup>4</sup> <https://www.astro.umontreal.ca/~bergeron/CoolingModels/>

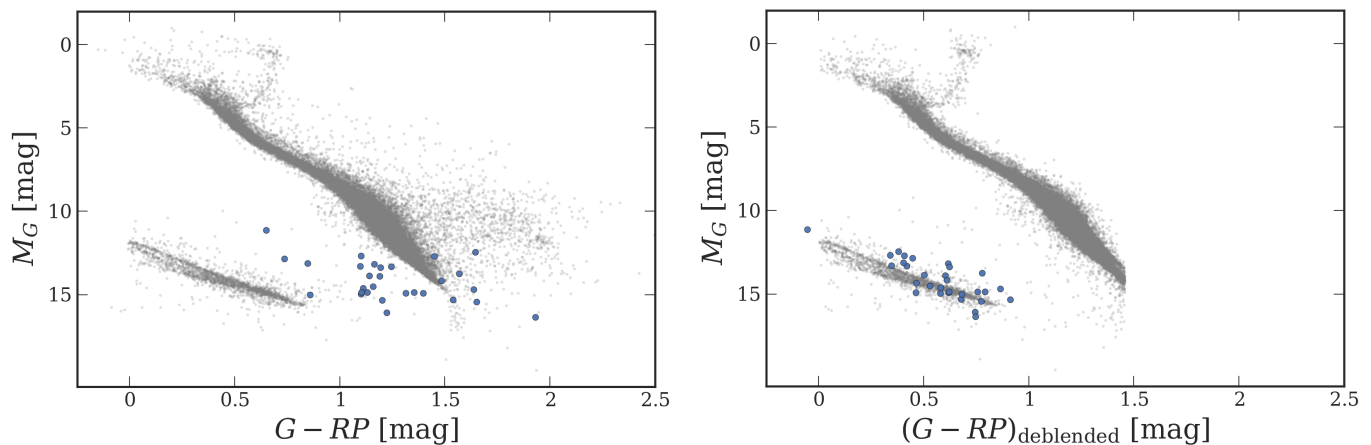


**Fig. 4.** Difference between the measured and de-blended  $G - RP$  colours for the identified white dwarfs and their location on the CMD. For comparison, the 50 pc *Gaia* DR3 sample is shown in the background (grey points); only objects with  $BP - RP$  colours in the range  $0.0 \text{ mag} < BP - RP < 4.25 \text{ mag}$  (the applicability range of the de-blending correction) are plotted. *Left:* CMD using the published  $G - RP$  colour. *Right:* CMD for the same sample, but using de-blended  $G - RP$  colour.

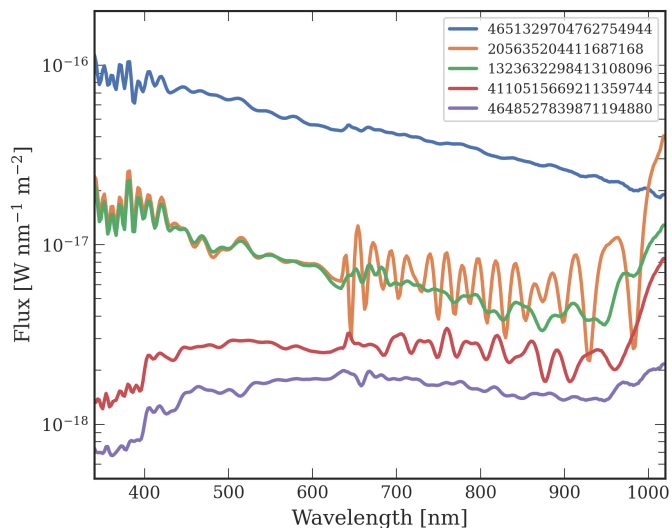


**Fig. 5.** Calibrated mean XP spectra for five white dwarfs in our sample. The corresponding *Gaia* DR3 source identifiers are indicated in the legend.

sample. Optionally, to allow for a much more reliable photometric fit, it can be supplemented with the distance, which in our case is derived from the *Gaia* DR3 parallax measurements, and the interstellar reddening. We did not apply any de-reddening corrections to the photometry, as it is reasonable to assume that the interstellar absorption within 50 pc is negligible. Thus, there is no degeneracy between  $T_{\text{eff}}$  and reddening – another advantage of nearby white dwarfs.

To infer the stellar parameters for objects with *Gaia* XP spectra, we used these spectra to derive synthetic photometry. For the remaining objects, we used  $G$ ,  $BP$ , and  $RP$  magnitudes from *Gaia* DR3, supplemented with PS1 photometry when available. In *Gaia*, the  $G$  and  $BP/RP$  magnitudes are obtained from two different instruments with different CCD window sizes. We note that although the blending can bias the measured values of the  $BP$  and  $RP$  fluxes, it results in only negligible changes in their  $BP - RP$  colour. Furthermore, the  $G$  band is less prone to blending due to the smaller window size of the *Gaia* astrometric field. In contrast to our selection criterion in Eq. (5), where we use

only the  $G$ -band magnitude and the  $BP - RP$  colour, here we also consider the  $BP$  and  $RP$  magnitudes separately to derive the stellar parameters. To minimise the impact of the blending on our analysis, we derived the de-blended  $G - RP$  colour, as fully described in Appendix B of Golovin et al. (2023), and used this value to correct the  $BP$  and  $RP$  magnitudes. The  $G$ -band magnitude and  $BP - RP$  colour were kept fixed. This correction is only applied to objects that do not have *Gaia* XP spectra. Fig. 4 displays CMDs before and after de-blending, illustrating the inconsistency in photometry and the power of the de-blending correction. Omitting de-blending would significantly impact the derived stellar parameters, resulting in, for instance, significantly underestimated masses of white dwarfs.

XP spectra in *Gaia* DR3 are available for five white dwarfs in our sample. These spectra are published in a ‘continuous’ form, where the coefficients of 55 basis functions, which are Gauss-Hermite polynomials, are provided. In Fig. 5, we present the mean sampled spectra obtained from the coefficients of the Gauss-Hermite polynomials. These spectra are then calibrated from internally calibrated mean spectra to the absolute system using the *GaiaXP* package. Sampling is performed from 340 nm to 1020 nm in steps of 2 nm. We note that the wiggles observed in the resulting spectra are not physical, but rather artefacts resulting from correlated errors of the polynomial coefficients.

Using these spectra, we computed synthetic photometry in various photometric systems, including *Gaia* DR3, Johnson-Kron-Cousins (JKC), PS1, and SDSS. However, we excluded the  $U_{\text{JKC}}$  and  $u_{\text{SDSS}}$  bands due to imperfections in the internal calibration process, as the XP spectra do not cover the bluest part of the transmission curves of these two bands.

Furthermore, it has been shown that the uncertainties of the synthetic fluxes are often underestimated and, to address this, we applied the empirical corrections to the uncertainties, following Gaia Collaboration et al. (2023); Montegriffo et al. (2023). Finally, we employed the derived spectral energy distribution to estimate the stellar parameters of the white dwarfs, considering only fluxes with a flux-over-error ratio greater than 10.

For each white dwarf, we report in Table 3 the DA and DB solutions for the inferred stellar parameters and their uncertainties. The distribution of the stellar parameters from both solutions derived in this work is shown in Fig. 6. There is a sig-

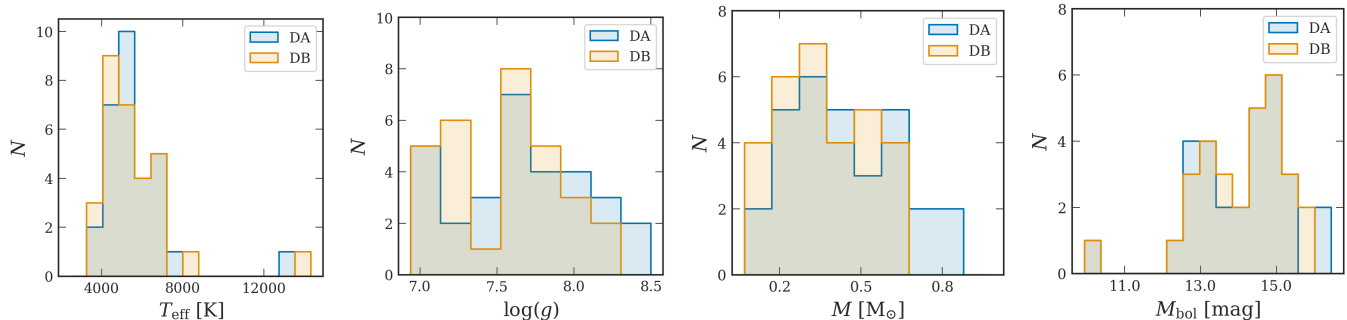


**Fig. 6.** Comparison of the distributions of stellar parameters derived in this work from DA and DB models, showing that there is substantial overlap between the two solutions. The DA solutions tend to have slightly higher values for both masses and surface gravities than the DB solutions, although in most cases the difference is not statistically significant.

nificant overlap between the distributions of the two solutions. While the derived masses and surface gravities generally tend to be slightly higher in the DA solutions than in the DB solutions, it is worth noting that this difference is not statistically significant for 90% of our sample.

The Montreal models, which we used to obtain the stellar parameters, assume a carbon-oxygen core for both DA and DB atmospheres. While we found a considerable number of white dwarfs with apparently low masses in our sample, it is crucial to note that such extremely low-mass white dwarfs are rare and are characterised by a helium-core composition (Althaus et al. 2013). Given that the main-sequence lifetime of low-mass stars can surpass the age of the Universe, the existence of extremely low-mass white dwarfs today suggests a formation process beyond single-star evolution, excluding cases of intense mass loss in high-metallicity stars (Kilic et al. 2007). Instead, the formation of extremely low-mass white dwarfs is anticipated to occur through binary evolution, involving one or more instances of common envelope evolution, as described in Li et al. (2019). The outcome of this binary evolution is manifested as a population of compact binary systems that have undergone significant changes, housing low-mass helium-core white dwarfs alongside their evolved companions. Importantly, there is currently no robust observational evidence supporting the existence of helium-core DB white dwarfs (Bergeron et al. 2011; Brown et al. 2020; Kosakowski et al. 2020). Furthermore, Sarna et al. (2000) have performed comprehensive calculations to elucidate the binary evolution for the formation of low-mass helium white dwarfs with stellar masses  $< 0.25 M_{\odot}$ . Their results show that after the detachment of the Roche lobe, the helium cores are enveloped by a substantial hydrogen layer with a mass ranging from 0.01 to 0.06  $M_{\odot}$ . Therefore, only low-mass DA white dwarfs are formed. Assuming that the mass values in our analysis are correct and not an artefact of photometric excess, we argue that the identified low-mass white dwarfs in our sample are most likely non-DBs.

Bergeron et al. (2019) noticed that there is a significant population of white dwarfs with apparently low masses ( $< 0.4 M_{\odot}$ ) positioned slightly above the densest part of the white dwarf sequence on the CMD. These objects were attributed by Bergeron et al. (2019) to unresolved double degenerate binaries. However, as can be seen in Fig. 2, the majority of the white dwarfs in our sample within this region are actually found in binaries with a main-sequence component. Given their small angular separation ( $\rho \leq 7.1''$ ) and the extreme difference in magnitude and sometimes also in colour between the components, it is plausible that the contamination of photometry, especially in the *BP* and *RP* bands, by a bright object in the field of view may also ac-

count for this effect. This conclusion gains further support from the fact that the white dwarfs in our sample with the unrealistically low estimated masses have the reddest CPM companions ( $BP - RP > 2.0$  mag) and the smallest angular separations ( $\rho < 3''$ ). Consequently, this raises concerns about the accuracy of the photometric masses in the presence of a bright, albeit well-resolved, companion in the vicinity of a white dwarf, and these masses should be interpreted with caution, as they may not be physically meaningful and can potentially cause a spurious excess in the white dwarf mass distribution at the low-mass end.

## 5. Improving the purity of the local white dwarf census: Contaminants in the 50 pc subsample of the GCWD21

The cut on the amplitude of the IPD GoF can be used to significantly improve not only the completeness but also the purity of the local white dwarf sample. This is achieved by eliminating the sources – hereafter referred to as contaminants – whose astrometric solutions fail to meet the criterion defined in Eq. (2) (see Fig. 7). By doing so we were able to identify a total of 103 contaminants among the 2338 high-confidence white dwarfs ( $P_{WD} > 0.75$ ) in the 50 pc subset of the GCWD21.

All identified contaminants are located at nominal distances greater than 25 pc. This is not entirely surprising, given that the total fraction of contaminants in *Gaia* DR3 is smaller for the 25 pc volume than the 50 pc volume. When considering the full range of absolute magnitudes and colours of the CMD, 11.78% of sources within 25 pc have spurious astrometry in *Gaia* DR3, whereas, within 50 pc, the fraction of sources with spurious astrometry increases to 50.84% (see Figs. 1 and A.2. in Golovin et al. 2023).

As shown in Fig. 8, the contaminants exhibit significantly larger absolute parallax uncertainties than confirmed white dwarfs, and they form two distinct populations in the  $(\sigma_{\varpi}, \varpi)$  parameter space. Parallax uncertainties of contaminants range from 0.50 mas to 4.28 mas, whereas parallax uncertainties of confirmed white dwarfs range from 0.01 mas to 0.93 mas. Among the 2235 confirmed white dwarfs, only 7 have parallax uncertainties above 0.50 mas, the minimum value observed for contaminants.

We note the presence of 9 sources with  $\varpi/\sigma_{\varpi} < 4$ . However, since they have  $\mu/\sigma_{\mu} > 10$ , they all fulfil one of the conditions listed in Eqs. 6, 12, or 19 in Gentile Fusillo et al. (2021). On the other hand, we found out that 3 115 of all 359 073 high-confidence white dwarfs in the GCWD21 (0.9% of the catalogue) have both  $\varpi/\sigma_{\varpi} < 4$  and  $\mu/\sigma_{\mu} \leq 10$ . These sources



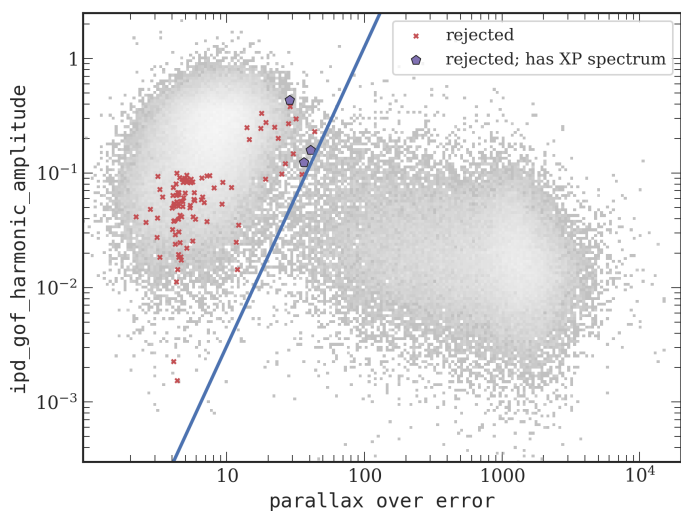


**Fig. 7.** Amplitude of the IPD GoF as a function of  $|\varpi/\sigma_\varpi|$  for the contaminants overplotted on the *Gaia* DR3 50 pc sample. Purple pentagon symbols indicate three contaminants with available XP spectra. The solid line corresponds to the cut described by Eq. (2).

are erroneously retained and will be removed from the catalogue in the next release based on *Gaia* DR3 (Gentile Fusillo, private communication).

Furthermore, the contaminants typically have much lower proper motion values than the confirmed white dwarfs, and their distributions differ significantly, as shown in Fig. 9. The majority of contaminants are located close to the Galactic bulge (Fig. 10).

Of the 103 contaminants, only three have an XP spectrum available in *Gaia* DR3. However, Fabricius et al. (2022) conclude that the XP spectra alone are not sufficient to correctly distinguish white dwarfs from other types of stellar sources. Nor can the reliability of an astrometric solution be inferred from these spectra. On the other hand, it is noteworthy that these three objects have particularly large RUWE values that range from 7.12 to 10.73. In fact, these are the objects with the largest RUWE values among all 103 contaminants. Furthermore, O’Brien et al. (2023) conducted spectroscopic follow-up observations of two contaminants from our sample: *Gaia* DR3 5681511931765351936, which has the largest amplitude of the IPD GoF as illustrated in Fig. 7, and *Gaia* DR3 4124294027400835584. Their observations revealed that both contaminants are main-sequence stars.

Finally, the position of the identified contaminants on the CMD (Fig. 11) coincides with the location of the sources classified as spurious in Rybizki et al. (2022, see their Fig. 18). Specifically, 97 out of 103 contaminants have an astrometric fidelity (fidelity\_v2) below 0.55 in Rybizki et al. (2022), supporting that their astrometric solutions are likely to be spurious. We note that the position of the identified contaminants on the CMD is also inconsistent with them being brown dwarfs. We argue that their astrometric solutions in *Gaia* DR3 are indeed spurious and that these contaminants should be excluded from the 50 pc sample, thereby improving the sample purity by 4.4%.

## 6. Discussion and conclusions

We have identified nine new white dwarfs and validated 21 previously reported white dwarf candidates within the 50 pc local population based on the astrometry and photometry from *Gaia* DR3. To eliminate sources with spu-

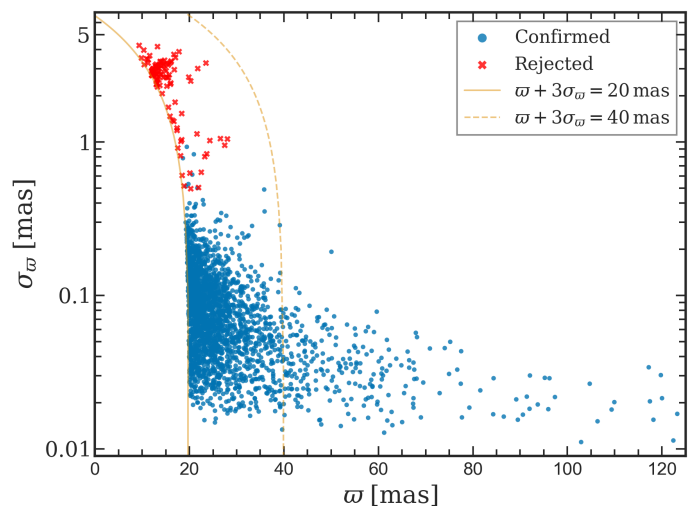


**Fig. 8.** Parallax uncertainty vs parallax for the contaminants (red symbols) and confirmed nearby white dwarfs (blue symbols). The dashed and the solid lines represent the 25 pc and 50 pc thresholds, respectively. The seven nearest confirmed white dwarfs are outside of the frame.

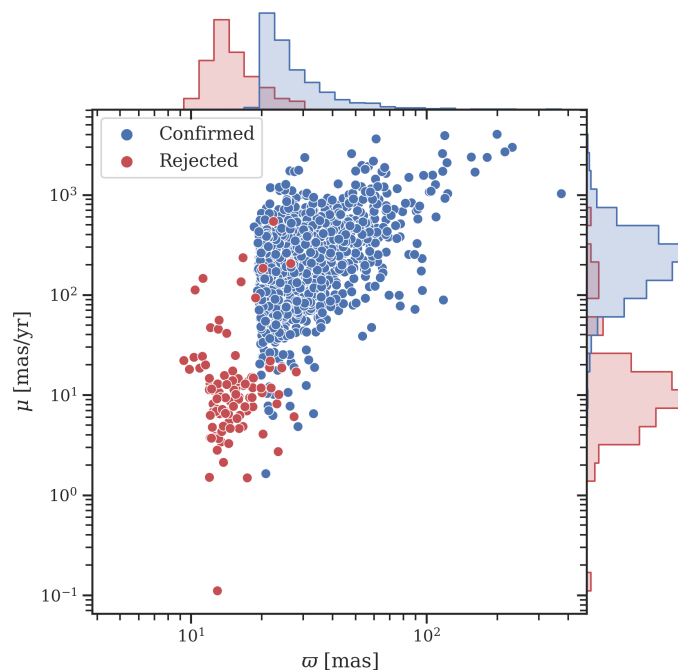


**Fig. 9.** Distributions of the total proper motions and parallaxes of the confirmed white dwarfs (blue symbols) and contaminants (red symbols) within 50 pc in the GCWD21.

rious astrometry, we used only two key parameters from *Gaia* DR3, namely *ipd\_gof\_harmonic\_amplitude* and *parallax\_over\_error*. Notably, we find that 20 white dwarfs, or two-thirds of our sample, have a CPM companion. At the same time, the identified white dwarfs are preferentially located close to the Galactic plane or in crowded fields. Fig. 12 shows the distribution of these white dwarfs in galactic coordinates. Of the 30 white dwarfs identified in this work, 14 are located within the region defined by  $|b| < 30^\circ$  and  $(0^\circ < l < 90^\circ$  or  $270^\circ < l < 360^\circ)$ . In this region, which covers one-quarter of the entire sky, a mere 7.5 stars would be statistically expected if they were uniformly distributed. In addition, three white dwarfs from

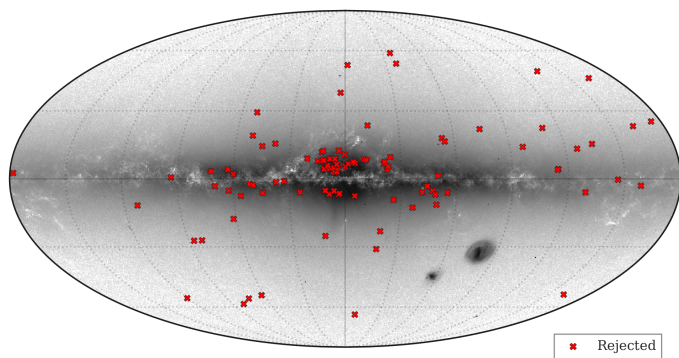


**Fig. 10.** Sky distribution of the contaminants in Galactic coordinates, with  $l = b = 0$  at the centre. The majority of contaminants are located in the vicinity of the Galactic bulge.

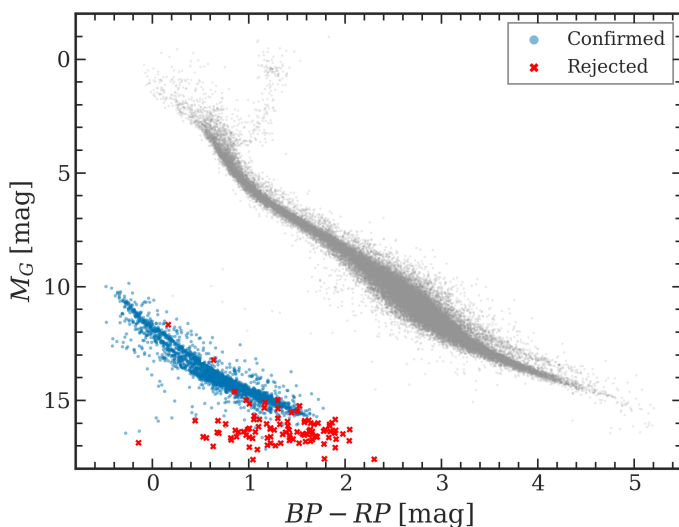


**Fig. 11.** *Gaia* DR3 CMD of the contaminants (red symbols) as compared against confirmed white dwarfs within 50 pc in the GCWD21 (blue symbols). For illustrative purposes, the CMD for the 50 pc *Gaia* DR3 sample is shown in the background (grey points).

our sample are located in the foreground of the Large Magellanic Cloud. The distribution of distances of the identified white dwarfs is shown in Fig. 13.

In our sample, we have identified a total of nine white dwarfs that, to the best of our knowledge, have not been previously reported as members of this class. Among these, one white dwarf (*Gaia* DR3 6013647666939138688) is within 25 pc. Additionally, two of the new white dwarfs have main-sequence CPM companions. While PS1 photometry is available for three of the new white dwarfs, further supporting their classification as white dwarfs, it also indicates that one of them may be one of the reddest white dwarfs in the solar neighbourhood.

The majority of the white dwarfs identified in this paper have been reported as nearby stars in the past. Among them, all four white dwarfs within 25 pc are by construction part of the CNS5, having been included during the catalogue compilation using the same selection criterion as in Eq. (2); however, no photometric signal-to-noise ratio threshold was enforced in the CNS5. The CNS5 catalogue, on the other hand, does not explicitly classify white dwarfs. Of the 30 identified white dwarfs, the GCNS lists 27 as nearby stars and rejects three, one of which is within 25 pc.

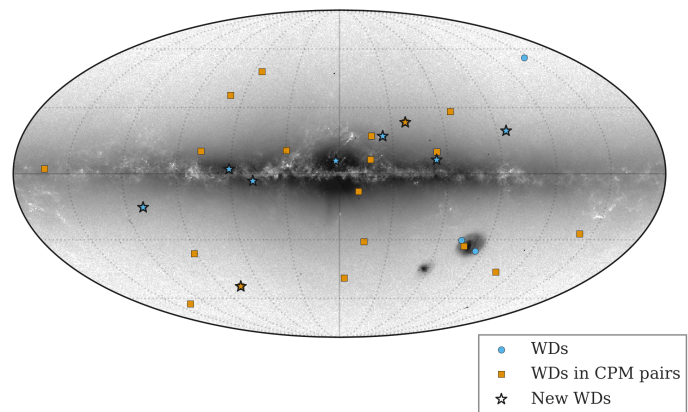


**Fig. 12.** Map of the identified white dwarfs (blue and orange symbols) in Galactic coordinates, with  $l = b = 0$  at the centre. Orange symbols represent objects with a CPM companion. A star symbol denotes each of the nine new white dwarfs presented in this paper. For comparison, the source density map for *Gaia* DR3 is shown in the background.

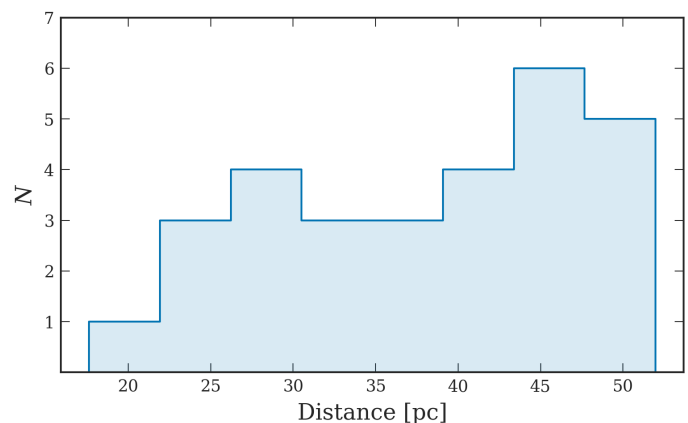


**Fig. 13.** Distribution of distances of the white dwarfs identified in this study.

As noted in the introduction to this paper, our selection validates 21 white dwarfs that have been previously documented as such at least once. However, these particular white dwarfs are missing from the GCWD21 and other recent volume-limited white dwarf samples. We argue that these objects are indeed white dwarfs with reliable *Gaia* DR3 astrometry and should therefore be included in such catalogues.

Within our sample, 18 objects have been classified as white dwarfs according to El-Badry et al. (2021), who compiled a catalogue of binary stars using *Gaia* EDR3 and categorised the components as either white dwarfs or main-sequence stars. However, it is worth noting that two objects from our sample (*Gaia* DR3 6119354336882826752 and *Gaia* DR3 2651214734078859648) are also present in the catalogue but have been misclassified as main-sequence stars due to an overly steep colour-magnitude cut employed in the study. El-Badry et al. (2021) designated any object not falling under the category of a white dwarf as a main-sequence star, which also included giants and subgiants. The quality cuts used in their study solely required a parallax-over-error ratio greater than 5, a parallax uncertainty of less than 2 mas, and a valid (non-null) value for the *G*-band magnitude.

The GCNS provides a parameter that indicates the probability of an object being a white dwarf. We consider an object with a

probability above 0.75 in the GCNS to be a reported white dwarf and do not count it as new in this paper. Remarkably, only three of the 27 catalogued white dwarfs have probabilities above 0.75, and only one of them has a probability above the 0.9 threshold. This discrepancy is most likely due to the effect of blending, which was not taken into account when the probabilities were derived.

Noteworthy is that our selection has rediscovered a white dwarf, *Gaia* DR3 4648527839871194880, previously reported by [Gentile Fusillo et al. \(2019\)](#) and with a 0.97 white dwarf probability in the GCNS but currently missing from the GCWD21 catalogue. Recently, this white dwarf was spectroscopically confirmed by [O’Brien et al. \(2023\)](#), who classified it as a magnetic DZH white dwarf. Using photometry from *Gaia* DR2, they also estimated its effective temperature to be  $T_{\text{eff}} = 4720 \pm 170$  K, with a surface gravity of  $\log(g) = 7.9 \pm 0.1$  dex. Our independent estimate, derived from *Gaia* XP spectroscopy and assuming a pure-hydrogen atmosphere, gives  $T_{\text{eff}} = 4666 \pm 22$  K and  $\log(g) = 7.81 \pm 0.02$  dex, in agreement with their values. The derivation of stellar parameters that are more realistic for a DZH white dwarf would require spectroscopy with a higher resolution and a higher signal-to-noise ratio to fit synthetic magnetic spectra to it (see e.g. [Külebi et al. 2009](#); [Hardy et al. 2023](#)).

Source density in *Gaia* DR3 correlates only weakly with the true source density on the sky, and consequently, it is a poor predictor of completeness, since one must also account for the *Gaia* selection function, as highlighted by [Cantat-Gaudin et al. \(2023\)](#). However, fields with a higher concentration of sources are more prone to blending and contamination, which affect the *BP* and *RP* bands even more strongly than the *G* band, leading to discrepancies in the photometry. Within our sample, all but eight sources have at least one other source in *Gaia* DR3 within a radius of  $4''$ . In the most extreme case (*Gaia* DR3 4314988445029569920), there are five other sources within this radius.

Furthermore, it is important to keep in mind that in *Gaia*, both telescopes project images onto the same CCD. Consequently, when one of the telescopes is pointed towards a crowded field, it inevitably influences the completeness and the selection function of the other field. Moreover, this can introduce peculiarities in the photometry of sources located within that field, even if it is not crowded. These peculiarities are often quantified through the photometric excess factor (phot\_bp\_rp\_excess\_factor in *Gaia* DR3; [Evans et al. 2018](#); [Lindegren et al. 2018](#); [Riello et al. 2021](#)). This factor is the dominant reason for the absence of the white dwarfs identified in this work from both the GCWD21 and the volume-limited samples listed in the introduction. All the white dwarfs in our sample have a highly significant flux excess in *Gaia* DR3, with  $C^*/\sigma_{C^*} > 37$ , where  $C^*$  is the corrected flux excess factor and  $\sigma_{C^*}$  is its dispersion for a sample of isolated stellar sources with good quality *Gaia* photometry, as defined in [Riello et al. \(2021\)](#). In [Jiménez-Esteban et al. \(2023\)](#), a  $3\sigma_{C^*}$  cut is applied, while [Gentile Fusillo et al. \(2021\)](#) use a  $5\sigma_{C^*}$  cut for sources in high-density fields and a  $|C^*| < 0.6$  cut for sources at high Galactic latitudes ( $|b| < 25$  deg) or low in low-density fields (density  $< 400$ )<sup>5</sup>.

The use of cuts on the RUWE is another reason why these white dwarfs have been rejected in prior studies. Within our sample, ten objects have  $\text{RUWE} > 1.4$ , while 20 objects have  $\text{RUWE} > 1.1$ , which is the threshold used in the GCWD21.

<sup>5</sup> The density parameter is defined in their paper as the total number of sources in *Gaia* EDR3 within  $50 \text{ arcsec}^2$  pixels.

Besides improving the overall completeness of the local white dwarf census, the identified white dwarfs are important objects for constraining the statistical properties of the solar neighbourhood. For example, four white dwarfs in our sample have an effective temperature of  $T_{\text{eff}} \leq 4000$  K within the  $1\sigma$  interval in either DA or DB solutions, and two of them have an absolute magnitude of  $M_G > 16.0$  mag. Such ultra-cool white dwarfs are extremely rare: only 24 white dwarfs within 50 pc with  $M_G > 16.0$  mag are listed in the GCWD21 (the contaminants are excluded). These objects define the faint end of the white dwarf luminosity function from which the age of the local stellar population can be inferred ([Schmidt 1959](#)).

In our sample, we have identified a total of 19 white dwarfs within binary or triple systems. Of these, one is a triple system in which the white dwarf (*Gaia* DR3 6017724140666000896) has a CPM companion (GJ 629) that is itself a spectroscopic binary. Additionally, one is a double white dwarf system (*Gaia* DR3 6039626481000400128 and *Gaia* DR3 6039626481009257472). The remaining binaries in our sample are Sirius-like systems, characterised by the presence of a significantly brighter main-sequence companion. Within our sample, the difference in brightness between the components of these systems ranges from 3.5 to 9.8 magnitudes in the *G* band.

One of the CPM companions of the white dwarfs validated in our study, GJ 3344, had been previously targeted in the spectroscopic search for undetected white dwarfs in binaries with main-sequence companions. [Bar et al. \(2017\)](#) selected 101 M dwarfs from the CNS3 catalogue ([Gliese & Jahreiß 1991](#)), limiting their sample to objects with strong near-UV emission, as detected by the GALEX survey ([Martin et al. 2005](#)). This near-UV emission can indicate the presence of an unresolved white dwarf companion. Despite their efforts, [Bar et al. \(2017\)](#) could not detect any white dwarfs around these 101 M dwarfs. The authors concluded that either the undetected white dwarfs are located outside the  $5''$  slit used for observations or the effective temperature of the undetected white dwarfs is below the detection limit, estimated to be  $8500 \sim 10000$  K for GJ 3344. For GJ 3344, both of these explanations could be valid, as (i) the targets in [Bar et al. \(2017\)](#) were positioned in the centre of the  $5''$  slit, while we found the white dwarf companion at a separation of  $\rho = 2.98''$ , and (ii) our estimation of its effective temperature from *Gaia* XP spectra suggests a value of about  $T_{\text{eff}} \sim 6700$  K.

Although the addition of these previously overlooked white dwarfs to the 50 pc sample has undoubtedly improved its completeness, the overall sample size has shrunk from 2338 to 2265 high-confidence white dwarfs. This reduction is a consequence of the improved sample purity achieved through the identification and exclusion of 103 sources with spurious astrometric solutions within the 50 pc subsample of the GCWD21. The distribution of the astrometric and photometric properties of these contaminants, along with their position in the sky, indicates that their astrometric solutions in *Gaia* DR3 are unreliable and that applying the cut on the amplitude of angular variation of the IPD GoF can significantly improve both the completeness and purity of the local white dwarf sample.

Furthermore, four white dwarfs identified in this study (three of them validated and one new) are located within 25 pc of the Sun. This is a significant addition (1.6%) to the 256 white dwarfs in the 25 pc sample of the GCWD21.

The identification of these new nearby white dwarfs is yet another step forward towards a volume-complete sample of white dwarfs.

Table 3. Stellar parameters for the white dwarfs listed in Table 1

Gaia DR3 source_id	DA solution										DB solution									
	$T_{\text{eff}}$ [K]	$\sigma_{T_{\text{eff}}}$ [K]	$\log(g)$ [dex]	$\sigma_{\log(g)}$ [dex]	$M$ [ $M_{\odot}$ ]	$\sigma_M$ [ $M_{\odot}$ ]	$M_{\text{bol}}$ [mag]	$\sigma_{M_{\text{bol}}}$ [mag]	$T_{\text{eff}}$ [K]	$\sigma_{T_{\text{eff}}}$ [K]	$\log(g)$ [dex]	$\sigma_{\log(g)}$ [dex]	$M$ [ $M_{\odot}$ ]	$\sigma_M$ [ $M_{\odot}$ ]	$M_{\text{bol}}$ [mag]	$\sigma_{M_{\text{bol}}}$ [mag]				
6013647666939138688	4326	180	8.4	0.1	0.83	0.09	16.11	0.04	4057	131	8.15	0.1	0.67	0.08	16.01	0.04				
4651329704762754944	6734	55	7.28	0.03	0.27	0.01	12.62	0.01	6723	55	7.25	0.03	0.24	0.01	12.67	0.01				
6017724140660000896	5038	245	8.08	0.17	0.64	0.12	14.96	0.06	4717	266	7.86	0.20	0.49	0.10	14.97	0.02				
2983256662868370048	7935	1789	7.62	0.51	0.31	0.16	12.39	0.12	8194	1389	7.69	0.36	0.29	0.16	12.43	0.14				
1938960722332184704	5633	106	8.24	0.05	0.74	0.04	14.71	0.01	5368	130	8.08	0.07	0.64	0.03	14.70	0.01				
2078105327586616832	4702	398	8.1	0.3	0.66	0.17	15.33	0.06	4436	411	7.9	0.3	0.53	0.17	15.32	0.04				
6119354336882826752	4167	47	7.04	0.06	0.17	0.02	14.62	0.01	4091	33	7.03	0.04	0.16	0.01	14.71	0.01				
2831490694928280576	6960	387	7.42	0.16	0.32	0.06	12.65	0.04	6841	375	7.3	0.2	0.28	0.06	12.70	0.04				
5956907713001974656	6857	188	7.86	0.07	0.51	0.05	13.28	0.02	6707	189	7.78	0.08	0.45	0.05	13.32	0.02				
6665685378201412992	5714	325	7.7	0.2	0.44	0.1	13.90	0.01	5480	350	7.55	0.2	0.36	0.11	13.93	0.01				
205635204411687168	6015	53	7.74	0.03	0.43	0.01	13.70	0.01	5812	59	7.60	0.04	0.36	0.02	13.73	0.01				
2651214734078859648	5008	75	7.05	0.08	0.18	0.02	13.75	0.02	4979	70	7.04	0.07	0.17	0.02	13.84	0.02				
4110515669211359744	4867	42	7.69	0.04	0.41	0.02	14.58	0.01	4494	42	7.39	0.04	0.28	0.02	14.64	0.01				
5463514273884166016	5087	66	7.52	0.05	0.34	0.02	14.19	0.01	4788	70	7.27	0.06	0.24	0.02	14.24	0.02				
4648527839871194880	4666	22	7.81	0.02	0.47	0.01	14.91	0.01	4323	21	7.54	0.02	0.33	0.01	14.96	0.01				
6566046912935892352	6596	527	7.27	0.24	0.26	0.09	12.68	0.05	6606	467	7.23	0.23	0.24	0.08	12.73	0.05				
6063480282704764928	3474	68	7.06	0.08	0.17	0.02	15.44	0.03	3626	28	7.03	0.04	0.16	0.01	15.25	0.02				
1355203232910297600	5586	96	7.05	0.07	0.19	0.02	13.20	0.01	5645	91	7.04	0.07	0.18	0.02	13.25	0.01				
2533660345315705344	13333	2526	7.7	0.2	0.45	0.12	10.14	0.38	13964	2714	7.8	0.3	0.49	0.18	10.06	0.36				
4663902104803506816	5040	72	8.04	0.05	0.61	0.03	14.90	0.02	4706	77	7.82	0.06	0.46	0.03	14.92	0.01				
3462945170562185088	4056	399	7.7	0.3	0.45	0.15	15.44	0.07	3914	253	7.53	0.27	0.35	0.13	15.39	0.04				
6080038412403680256	5370	80	7.05	0.07	0.19	0.02	13.40	0.01	5398	66	7.04	0.05	0.17	0.02	13.46	0.01				
2021862490380335232	5969	338	8.22	0.16	0.73	0.11	14.41	0.03	5737	370	8.09	0.19	0.62	0.11	14.41	0.03				
6039626481000400128	5554	102	8.12	0.06	0.67	0.04	14.59	0.01	5277	116	7.95	0.07	0.54	0.04	14.59	0.01				
6039626481009257472	5241	308	7.9	0.2	0.55	0.1	14.55	0.05	4923	334	7.7	0.25	0.4	0.1	14.58	0.02				
4837326390227065344	6286	308	7.6	0.15	0.39	0.07	13.33	0.02	6106	318	7.5	0.18	0.32	0.07	13.37	0.02				
1323632298413108096	6856	53	7.59	0.02	0.38	0.01	12.93	0.01	6755	53	7.53	0.03	0.34	0.01	12.98	0.01				
4468278954501360128	4522	72	7.54	0.08	0.34	0.03	14.74	0.02	4182	71	7.23	0.09	0.22	0.03	14.79	0.02				
625602672887745152	4384	94	7.51	0.09	0.33	0.04	14.85	0.01	4121	79	7.26	0.09	0.24	0.03	14.89	0.01				
4314988445029569920	3677	572	8.0	0.5	0.6	0.2	16.25	0.2	3646	407	7.7	0.4	0.5	0.2	16.0	0.15				

**Acknowledgements.** We would like to thank the anonymous referee for a thorough review and many helpful comments, which have improved this manuscript. Part of this work was supported by the International Max Planck Research School for Astronomy and Cosmic Physics at the University of Heidelberg, IMPRS-HD, Germany. A.G. and A.J. gratefully acknowledge funding from the Deutsche Forschungsgemeinschaft (DFG, German Research Foundation) – Project-ID 138713538 – SFB 881 (“The Milky Way System”, subproject A06). This work has made use of: TOPCAT (Taylor 2005, 2019), a GUI analysis package for working with tabular data in astronomy; Astropy, a community-developed core Python package for Astronomy (Astropy Collaboration et al. 2018); Scipy, a set of open source scientific and numerical tools for Python (Virtanen et al. 2020); WDPHOTools (Lam et al. 2022), a white dwarf photometric toolkit in Python; GaiaXPy (Gaia Collaboration et al. 2023), a Python package, developed and maintained by members of the *Gaia* Data Processing and Analysis Consortium (DPAC), and in particular, Coordination Unit 5 (CU5), and the Data Processing Centre located at the Institute of Astronomy, Cambridge, UK (DPCI), the VizieR catalogue access tool and the SIMBAD database operated at CDS, Strasbourg, France; the National Aeronautics and Space Administration (NASA) Astrophysics Data System (ADS). This work has made use of data from the European Space Agency (ESA) mission *Gaia* (<https://www.cosmos.esa.int/gaia>), processed by the *Gaia* Data Processing and Analysis Consortium (DPAC, <https://www.cosmos.esa.int/web/gaia/dpac/consortium>). Funding for the DPAC has been provided by national institutions, in particular, the institutions participating in the *Gaia* Multilateral Agreement. The Pan-STARRS1 Surveys (PS1) have been made possible through contributions of the Institute for Astronomy, the University of Hawaii, the Pan-STARRS Project Office, the Max-Planck Society and its participating institutes, the Max Planck Institute for Astronomy, Heidelberg and the Max Planck Institute for Extraterrestrial Physics, Garching, The Johns Hopkins University, Durham University, the University of Edinburgh, Queen’s University Belfast, the Harvard-Smithsonian Center for Astrophysics, the Las Cumbres Observatory Global Telescope Network Incorporated, the National Central University of Taiwan, the Space Telescope Science Institute, the National Aeronautics and Space Administration under Grant No. NNX08AR22G issued through the Planetary Science Division of the NASA Science Mission Directorate, the National Science Foundation under Grant No. AST-1238877, the University of Maryland, and Eotvos Lorand University (ELTE).

## References

- Althaus, L. G., Miller Bertolami, M. M., & Córscico, A. H. 2013, *A&A*, 557, A19  
 Astropy Collaboration, Price-Whelan, A. M., Sipőcz, B. M., et al. 2018, *AJ*, 156, 123  
 Bar, I., Vreeswijk, P., Gal-Yam, A., Ofek, E. O., & Nelemans, G. 2017, *ApJ*, 850, 34  
 Bédard, A., Bergeron, P., Brassard, P., & Fontaine, G. 2020, *ApJ*, 901, 93  
 Bergeron, P., Dufour, P., Fontaine, G., et al. 2019, *ApJ*, 876, 67  
 Bergeron, P., Wesemael, F., Dufour, P., et al. 2011, *ApJ*, 737, 28  
 Bopp, B. W., Evans, D. S., Laing, J. D., & Deeming, T. J. 1970, *MNRAS*, 147, 355  
 Brown, W. R., Kilic, M., Kosakowski, A., et al. 2020, *ApJ*, 889, 49  
 Busso, G., Cacciari, C., Bellazzini, M., et al. 2021, *Gaia* EDR3 documentation Chapter 5: Photometric data, *Gaia* EDR3 documentation  
 Cantat-Gaudin, T., Fouesneau, M., Rix, H.-W., et al. 2023, *A&A*, 669, A55  
 Catalán, S., Isern, J., García-Berro, E., & Ribas, I. 2008, *MNRAS*, 387, 1693  
 Chambers, K. C., Magnier, E. A., Metcalfe, N., et al. 2016, arXiv e-prints, arXiv:1612.05560  
 Creevey, O. L., Sordo, R., Paillet, F., et al. 2023, *A&A*, 674, A26  
 Cukanovaite, E., Tremblay, P. E., Toonen, S., et al. 2023, *MNRAS*, 522, 1643  
 De Silva, G. M., Freeman, K. C., Bland-Hawthorn, J., et al. 2015, *MNRAS*, 449, 2604  
 Dufour, P., Blouin, S., Couto, S., et al. 2017, in *Astronomical Society of the Pacific Conference Series*, Vol. 509, 20th European White Dwarf Workshop, ed. P. E. Tremblay, B. Gänsicke, & T. Marsh, 3  
 El-Badry, K., Rix, H.-W., & Heintz, T. M. 2021, *MNRAS*, 506, 2269  
 Evans, D. W., Riello, M., De Angeli, F., et al. 2018, *A&A*, 616, A4  
 Fabricius, C., Babusiaux, C., Luri, X., et al. 2022, *Gaia* DR3 documentation Chapter 14: Validation, *Gaia* DR3 documentation, European Space Agency  
 Fabricius, C., Luri, X., Arenou, F., et al. 2021, *A&A*, 649, A5  
 Ferrario, L. 2012, *MNRAS*, 426, 2500  
 Fleury, L., Caiazzo, I., & Heyl, J. 2022, *MNRAS*, 511, 5984  
 Fuhrmann, K., Chini, R., Kaderhandt, L., & Chen, Z. 2017, *ApJ*, 836, 139  
 Gaia Collaboration, Brown, A. G. A., Vallenari, A., et al. 2021a, *A&A*, 649, A1  
 Gaia Collaboration, Montegriffo, P., Bellazzini, M., et al. 2023, *A&A*, 674, A33  
 Gaia Collaboration, Smart, R. L., Sarro, L. M., et al. 2021b, *A&A*, 649, A6  
 Gentile Fusillo, N. P., Tremblay, P. E., Cukanovaite, E., et al. 2021, *MNRAS*, 508, 3877  
 Gentile Fusillo, N. P., Tremblay, P.-E., Gänsicke, B. T., et al. 2019, *MNRAS*, 482, 4570  
 Gliese, W. & Jahreiß, H. 1991, Preliminary Version of the Third Catalogue of Nearby Stars, On: The Astronomical Data Center CD-ROM: Selected Astronomical Catalogs  
 Golovin, A., Reffert, S., Just, A., et al. 2023, *A&A*, 670, A19  
 Halbwachs, J.-L., Pourbaix, D., Arenou, F., et al. 2023, *A&A*, 674, A9  
 Hardy, F., Dufour, P., & Jordan, S. 2023, *MNRAS*, 520, 6111  
 Harris, H. C., Munn, J. A., Kilic, M., et al. 2006, *AJ*, 131, 571  
 Holl, B., Fabricius, C., Portell, J., et al. 2023a, *A&A*, 674, A25  
 Holl, B., Sozzetti, A., Sahlmann, J., et al. 2023b, *A&A*, 674, A10  
 Isern, J. 2019, *ApJ*, 878, L11  
 Isern, J., García-Berro, E., Torres, S., & Catalán, S. 2008, *ApJ*, 682, L109  
 Jiménez-Esteban, F. M., Torres, S., Rebassa-Mansergas, A., et al. 2023, *MNRAS*, 518, 5106  
 Kaltenegger, L. & Faherty, J. K. 2021, *Nature*, 594, 505  
 Kilic, M., Stanek, K. Z., & Pinsonneault, M. H. 2007, *ApJ*, 671, 761  
 Kosakowski, A., Kilic, M., Brown, W. R., & Gianninas, A. 2020, *ApJ*, 894, 53  
 Kőlebi, B., Jordan, S., Euchner, F., Gänsicke, B. T., & Hirsch, H. 2009, *A&A*, 506, 1341  
 Lam, M. C., Yuen, K. W., Green, M. J., & Li, W. 2022, *RAS Techniques and Instruments*, 1, 81  
 Li, Z., Chen, X., Chen, H.-L., & Han, Z. 2019, *ApJ*, 871, 148  
 Liebert, J., Dahn, C. C., Gresham, M., & Strittmatter, P. A. 1979, *ApJ*, 233, 226  
 Liebert, J., Dahn, C. C., & Monet, D. G. 1988, *ApJ*, 332, 891  
 Lindegren, L. 2018, *Gaia* Data Processing and Analysis Consortium (DPAC) technical note GAIA-C3-TN-LU-LL-124-01, available at <https://www.cosmos.esa.int/web/gaia/public-dpac-documents>  
 Lindegren, L., Hernández, J., Bombrun, A., et al. 2018, *A&A*, 616, A2  
 Lindegren, L., Klioner, S. A., Hernández, J., et al. 2021, *A&A*, 649, A2  
 Martin, D. C., Fanson, J., Schiminovich, D., et al. 2005, *ApJ*, 619, L1  
 McGill, P., Anderson, J., Casertano, S., et al. 2023, *MNRAS*, 520, 259  
 McGill, P., Smith, L. C., Evans, N. W., Belokurov, V., & Smart, R. L. 2018, *MNRAS*, 478, L29  
 Montegriffo, P., De Angeli, F., Andrae, R., et al. 2023, *A&A*, 674, A3  
 O’Brien, M. W., Tremblay, P. E., Gentile Fusillo, N. P., et al. 2023, *MNRAS*, 518, 3055  
 Pecaut, M. J. & Mamajek, E. E. 2013, *ApJS*, 208, 9  
 Pourbaix, D., Arenou, F., Gavras, P., et al. 2022, *Gaia* DR3 documentation Chapter 7: Non-single stars, *Gaia* DR3 documentation, European Space Agency  
 Pourbaix, D., Tokovinin, A. A., Batten, A. H., et al. 2004, *A&A*, 424, 727  
 Raghavan, D., McAlister, H. A., Henry, T. J., et al. 2010, *ApJS*, 190, 1  
 Reylé, C., Jardine, K., Fouqué, P., et al. 2023, in *The 21st Cambridge workshop on Cool Stars, Stellar Systems, and the Sun*, Toulouse, France, 2022, ed. A. S. Brun, J. Bouvier, & P. Petit, arXiv:2302.02810  
 Riello, M., De Angeli, F., Evans, D. W., et al. 2021, *A&A*, 649, A3  
 Rowell, N. 2013, *MNRAS*, 434, 1549  
 Rybizki, J., Green, G. M., Rix, H.-W., et al. 2022, *MNRAS*, 510, 2597  
 Sarna, M. J., Ergma, E., & Gerškevičš-Antipova, J. 2000, *MNRAS*, 316, 84  
 Schmidt, M. 1959, *ApJ*, 129, 243  
 Scholz, R. D. 2020, *A&A*, 637, A45  
 Spaeth, D., Reffert, S., Trifonov, T., & Golovin, A. 2023, *Research Notes of the American Astronomical Society*, 7, 12  
 Steinmetz, M., Matijević, G., Enke, H., et al. 2020, *AJ*, 160, 82  
 Taylor, M. B. 2005, in *Astronomical Society of the Pacific Conference Series*, Vol. 347, *Astronomical Data Analysis Software and Systems XIV*, ed. P. Shopbell, M. Britton, & R. Ebert, 29  
 Taylor, M. B. 2019, in *Astronomical Society of the Pacific Conference Series*, Vol. 523, *Astronomical Data Analysis Software and Systems XXVII*, ed. P. J. Teuben, M. W. Pound, B. A. Thomas, & E. M. Warner, 43  
 Torres, S., Canals, P., Jiménez-Esteban, F. M., Rebassa-Mansergas, A., & Solano, E. 2022, *MNRAS*, 511, 5462  
 Torres, S., Cruz, P., Murillo-Ojeda, R., et al. 2023, *A&A*, 677, A159  
 Ulla, A., Creevey, O. L., Álvarez, M. A., et al. 2022, *Gaia* DR3 documentation Chapter 11: Astrophysical parameters, *Gaia* DR3 documentation, European Space Agency  
 Vincent, O., Bergeron, P., & Dufour, P. 2023, *MNRAS*, 521, 760  
 Virtanen, P., Gommers, R., Oliphant, T. E., et al. 2020, *Nature Methods*, 17, 261  
 Yanny, B., Rockosi, C., Newberg, H. J., et al. 2009, *AJ*, 137, 4377  
 Yuan, J. W. 1992, *A&A*, 261, 105

## Appendix A: Discrete source classifier (DSC) in *Gaia* DR3

One of the key data products within *Gaia* DR3 is the `astrophysical_parameters` table, which provides, among other information, the probabilistic classification of sources into several classes, including white dwarfs. Specifically for white dwarfs, the DSC uses two classifiers: `specmod`, which provides probabilities derived from XP spectra, and `combmod`, which combines spectroscopic probabilities with those obtained from astrometry and photometry.

All of the white dwarfs identified in this study have posterior class probabilities below 0.5. The probability values range from  $2 \times 10^{-12}$  to 0.46 in `combmod`, and from 0 to 0.04 in `specmod`. In addition, one white dwarf (*Gaia* DR3 1938960722332184704) is excluded from the classifier.

Previously it has been shown that the DSC probabilities for white dwarfs and binaries may be poorly calibrated and consequently due to the poor performance of the classifier (with a purity of only about 25%) the use of these probabilities to construct samples of such objects is not recommended (Creevey et al. 2023; Ulla et al. 2022). This limitation becomes apparent when analysing the CMD colour-coded with white dwarf probabilities (see Fig. A.1). In particular, in most cases, only objects in the upper part of the white dwarf sequence have probabilities greater than 0.5. What is striking is that the sharp decrease in the derived probabilities occurs at about  $BP - RP = 0.6$ , corresponding to the colour where the *RP* flux starts to exceed the *BP* flux.

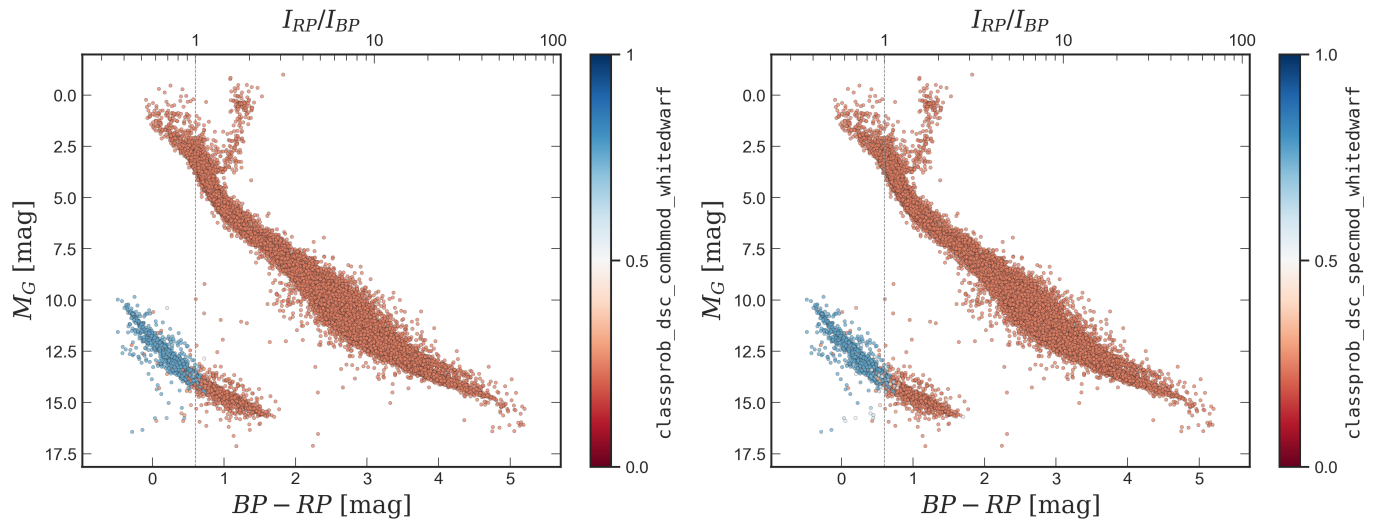


**Fig. A.1.** CMD for the 50 pc sample colour-coded with the probability of being a white dwarf as listed in *Gaia* DR3. The dashed line indicates the colour at which the  $BP$  and  $RP$  fluxes are equal. *Left*: probability derived from XP-spectroscopy, photometry, and astrometry (DSC-Combmod classifier). *Right*: probability derived from XP-spectroscopy only (DSC-Specmod classifier).